Disentangling multidimensional femtosecond spectra of excitons by pulse shaping with coherent control

Darius Abramavicius and Shaul Mukamel[a]

Department of Chemistry, University of California, Irvine, California 92697

Sequences of carefully timed and shaped optical pulses provide femtosecond snapshots of molecular structure as well as electronic and vibrational dynamical processes, in analogy with multidimensional NMR. We apply a genetic learning algorithm towards the design of pulse sequences which simplify the multidimensional signals by controlling the relative intensities of various peaks. Numerical simulations demonstrate how poorly resolved weak features may be amplified and observed by using optimized optical pulses, specifically shaped to achieve a desired spectroscopic target. © *2004 American Institute of Physics.* [DOI: 10.1063/1.1691020]

I. INTRODUCTION

Elaborate NMR pulse sequences are currently routinely used in structure determination of complex biomolecules.[1,2] Recent progress in optical pulse shaping[3–9] has opened up the possibility of extending these techniques towards the study of electronic and vibrational motions in molecules.[10–15] The interpretation of NMR measurements is facilitated by the relative simplicity of spin Hamiltonians which often allow back of the envelope, perturbative, design of new pulse sequences.[16] Vibrational and electronic motions are far more complex than spins,[12,17] and developing optical or infrared pulse sequences generally requires elaborate and expensive simulations.

In this paper we demonstrate how a genetic pulse-shaping algorithm may be employed towards the optimization of multidimensional signals. Introducing coherent-control ideas into multidimensional spectroscopy provides a new tool, that could make high-resolution ultrafast snapshots of complex biomolecules a reality. The field of coherent control has been driven by the objective of selectively breaking and making chemical bonds.[18–20] The primary goal has been to guide chemical reactions to a desired product using laser pulses, leading to the formation of novel stable or metastable molecules.[21,22] Other applications of coherent control were directed towards the manipulation of current echoes in semiconductors,[23] energy flow in light harvesting complexes,[24] and vibrational wave packets.[25] Nonlinear optics applications include two-photon transitions,[26,27] soft x-ray emission,[28] and four-wave mixing (coherent Raman) spectroscopy and microscopy[29,30] where the elimination of nonresonant background and the selective excitation of closely-lying Raman modes was achieved.

The proposed application of closed-loop learning optimization algorithms for the design of optical pulses has provided a major advance towards the practical implementation of control techniques in complex molecular systems.[31] The implementation of the idea involves three elements: (i) an input trial laser pulse, (ii) applying the pulse to the sample and observing the signal, (iii) using a genetic learning algorithm to generate new pulse shapes based on these prior experiments.[32] These steps are repeated until the desired target is achieved. Genetic algorithms perform a parallel search on an entire ''population'' of pulses, use payoff (cost function) information, rather than derivatives or other auxiliary knowledge, and employ probabilistic, rather than deterministic, rules. The necessary population size is typically much smaller compared to Monte Carlo simulations. Various pulse shaping schemes with genetic optimization were studied recently by Zeidler *et al.*[33]

Multidimensional spectroscopy is based on an elementary nonlinear optical process known as *four-wave mixing*. Consider a molecule interacting with three monochromatic optical fields with frequencies ω_a, ω_b, ω_c and polarized along the directions α, β, γ, respectively (which assume the values x, y, z). The three beams mix by their coupling with the molecule to generate a new signal field with frequency ω_s and polarization σ. The amplitude of this field, calculated perturbatively in the incoming fields, is proportional to the third order nonlinear susceptibility tensor $\chi^{(3)}_{\sigma\alpha\beta\gamma}(-\omega_s;\omega_a,\omega_b,\omega_c)$.

Generally $\chi^{(3)}$ has $8\times6\times81$ contributions (8 Liouville-space pathways, six permutations of the three frequencies, and 81 tensor components). Each contribution further involves a fourfold summation over molecular eigenstates.[34] $\chi^{(3)}$ is thus determined by strong interferences among the various contributions. Using laser pulses defined by the envelope $\mathcal{E}_\alpha(\mathbf{r},\omega) \equiv \int dt E_\alpha(\mathbf{r},t)\exp(i\omega t)$, where $\alpha = x$, y, z denotes the polarization, the signal will be proportional to the σth component of the induced polarization which is given by[34]

---

[a]Author to whom correspondence should be addressed. Telephone: 949-824-7600; Fax: 949-824-8571. Electronic mail: smukamel@uci.edu

8373

$$P_\sigma^{(3)}(\mathbf{r},t)=\sum_{\alpha\beta\gamma}\int\int\int d\omega_s d\omega_a d\omega_b d\omega_c \exp(-i\omega_s t)$$

$$\times\chi_{\sigma\alpha\beta\gamma}^{(3)}(-\omega_s;\omega_a,\omega_b,\omega_c)$$

$$\times\mathcal{E}_\alpha(\mathbf{r},\omega_a)\mathcal{E}_\beta(\mathbf{r},\omega_b)\mathcal{E}_\gamma(\mathbf{r},\omega_c). \tag{1}$$

In a frequency-domain experiment, $\mathcal{E}_\alpha(\mathbf{r},\omega_a)$ is a narrowly peaked function of frequency and the integrations in Eq. (1) can be eliminated so that $P_\sigma^{(3)}(\mathbf{r},\omega_s)$ is directly proportional to $\chi_{\sigma\alpha\beta\gamma}^{(3)}(-\omega_s;\omega_a,\omega_b,\omega_c)$. The multiple integrations over pulse envelopes in Eq. (1) imply that $P_\sigma^{(3)}(\mathbf{r},t)$ is given by a *coherent superposition* of the various frequency components of $\chi^{(3)}$ which may be externally controlled by the pulse envelopes. $P_\sigma^{(3)}$ is thus affected by two types of interference: those contained in $\chi^{(3)}$ and those resulting from the multiple integrations (coherent superpositions of various frequency components). Pulse shaping[3–6,8,9] offers numerous possibilities for affecting the signal by controlling the latter interferences. These will be the focus of the present study.

We shall consider a four wave mixing process carried out with three incoming fields ($j=1,2,3$) and a fourth field ($j=4$) associated with the heterodyne detection: $\mathbf{E}(\mathbf{r},t)=\sum_{j=1}^{4}\sum_\alpha E_{j\alpha}(t-\bar{\tau}_j)\exp[i(\mathbf{k}_j\mathbf{r})-i\bar{\omega}_j t]+\text{c.c.}$ Here $E_{j\alpha}(t-\bar{\tau}_j)$ is a complex envelope function (slowly-varying compared to the optical period $2\pi/\bar{\omega}_j$). $\mathbf{k}_j$, $\bar{\omega}_j$, and $\bar{\tau}_j$ are the wave vector, carrier frequency, and peak time of the jth mode, respectively. The frequency domain amplitude of the field is given by

$$\mathcal{E}_\alpha(\mathbf{r},\omega)=\sum_{j=1}^{4}\mathcal{E}_{j\alpha}(\omega-\bar{\omega}_j)\exp\{i\mathbf{k}_j\mathbf{r}+i(\omega-\bar{\omega}_j)\bar{\tau}_j$$

$$+i\phi_{j\alpha}(\omega-\bar{\omega}_j)\}+\text{c.c.}, \tag{2}$$

where $\mathcal{E}_{j\alpha}(\omega)\exp(i\phi_{j\alpha}(\omega))$ is the Fourier transform of the envelope $E_{j\alpha}(t)$. Both the envelope function $\mathcal{E}_{j\alpha}$ and its phase $\phi_{j\alpha}$ are taken to be real.

The heterodyne signal involves interference between the polarization and the heterodyne field ($E_{4\alpha}(\tau)$), and is given by[17,34]

$$S(\mathbf{k}_s)=\text{Re}\sum_{\sigma,\alpha,\beta,\gamma}\int\int\int d\omega_s d\omega_a d\omega_b d\omega_c$$

$$\times\chi_{\sigma\alpha\beta\gamma}^{(3)}(-\omega_s,\omega_a,\omega_b,\omega_c)\mathcal{E}_{1\alpha}(\omega_a-\bar{\omega}_1)$$

$$\times\mathcal{E}_{2\beta}(\omega_b-\bar{\omega}_2)\mathcal{E}_{3\gamma}(\omega_c-\bar{\omega}_3)$$

$$\times\mathcal{E}_{4\sigma}(\omega_s-\bar{\omega}_4)\exp(i\kappa_{\sigma\alpha\beta\gamma}^{(s)}). \tag{3}$$

The only possible directions of the signal are $\mathbf{k}_s=u\mathbf{k}_1+v\mathbf{k}_2+w\mathbf{k}_3$, where u, v, and w are integers ($=0,\pm1,\pm2,...$).[34] The phase $\kappa_{\sigma\alpha\beta\gamma}^{(s)}$ which depends on $\mathbf{k}_s$ is $\kappa_{\sigma\alpha\beta\gamma}^{(s)}=u\Phi_{1\alpha}(\omega_a)+v\Phi_{2\beta}(\omega_b)+w\Phi_{3\gamma}(\omega_c)-\Phi_{4\sigma}(\omega_s)$, where the phase functions are given by $\Phi_{j\alpha}(\omega)=\phi_{j\alpha}(\omega-\bar{\omega}_j)+(\omega-\bar{\omega}_j)\bar{\tau}_j$ with $j=1,2,3,4$. Each choice of integers u, v, and w represents a distinct technique. When the pulses are very short and well separated, $\mathbf{k}_1$ comes first, followed by $\mathbf{k}_2$ and finally $\mathbf{k}_3$. However, Eq. (3) is not limited to this case and any time ordering is permitted. The signal depends on the observation direction $\mathbf{k}_s$ as well as all the
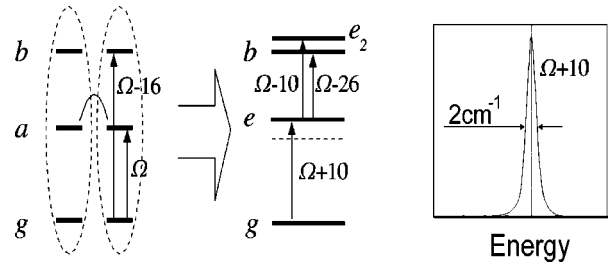

FIG. 1. Model dimer of three level molecules, representing either electronic excitations or anharmonic vibrations. $|g\rangle$, $|a\rangle$, and $|b\rangle$ indicate ground, first, and second excited states of individual chromophores. Molecular excited states are defined as follows: First excited state energy equal to $\Omega_{ma}=\Omega=1677\text{ cm}^{-1}$ ($m=1,2$; $a=1$) and the first overtone energy $\Omega_{mb}=2\Omega-16=3338\text{ cm}^{-1}$ ($m=1,2$; $b=2$). The dipole–dipole coupling between the excited molecular states is assumed as $J_{ma,na}=10\text{ cm}^{-1}$ ($a=1$, $m\neq n$). The coupling with the second excited states is neglected ($J_{ma,nb}=0$; $a=2$, $m\neq n$). The transition dipole moments are parallel and $\mu_{m,ab}=\sqrt{2}\mu_{ma}$. In the eigenstate representation $|e\rangle$ and $|e_2\rangle$ indicate one-exciton state and two-exciton state, respectively. The overtone states are the same in exciton basis in our model. Possible optical transitions and the linear absorption spectrum is shown as well.

parameters specifying the different pulses such as the envelopes $\mathcal{E}_{j\alpha}(\omega)$, $\phi_{j\alpha}(\omega)$, $\bar{\omega}_j$, $\bar{\tau}_j$, etc. This large parameter space may be explored and optimized to achieve desired spectroscopic objectives.

Our model system of coupled localized vibrations (or electronic excitations of molecular aggregates) is introduced in Sec. II. Simulations of two-dimensional spectra presented in Sec. III show how the intensities of different peaks may be independently controlled by pulse shaping, allowing us to observe new, otherwise unresolved, spectral features. Our results are discussed in Sec. IV. Details of the pulse shaping algorithm are given in the Appendix.

II. THE NONLINEAR RESPONSE OF EXCITONS

We consider the system of coupled localized anharmonic vibrations shown in Fig. 1. The vibrational modes are labeled $m, n,...,$ and the states are g (ground state) and excited states a, b, c,.... The eigenstates of this system are known as excitons. The same model of coupled multilevel chromophores can also represent electronic excitations of aggregates,[35] but for clarity we focus on vibrations.

To describe the system we introduce creation ($\hat{B}_{ma}^\dagger\equiv|ma\rangle\langle mg|$) and annihilation ($\hat{B}_{ma}\equiv|mg\rangle\langle ma|$) operators, which create/annihilate the excited state $|a\rangle$ on the mth chromophore, $|mg\rangle$ being its ground state. The Hamiltonian has three terms: $\hat{H}=\hat{H}_S+\hat{H}_{SB}-\hat{\mathbf{P}}\cdot\mathbf{E}(\mathbf{r},t)$. $\hat{H}_S$ represents the coupled chromophores

$$\hat{H}_S=\sum_{m,a}\Omega_{ma}\hat{B}_{ma}^\dagger\hat{B}_{ma}+\sum_{m,a,n,b}^{m\neq n}J_{ma,nb}\hat{B}_{ma}^\dagger\hat{B}_{nb}, \tag{4}$$

where Ω_{ma} are the chromophore energies and $J_{ma,nb}$ their couplings. $\hat{H}_{SB}$ represents the interaction with a thermal bath,

$$\hat{H}_{SB}=\sum_{m,a}\hat{B}_{ma}^\dagger\hat{B}_{ma}q_{ma}^{(C)}, \tag{5}$$

where $q_{ma}^{(C)}$ is a collective bath coordinate which modulates the chromophore energies and represents the coupling strength between state a of the mth chromophore and the bath. This coupling is linear in the bath coordinate which induces fluctuations in the diagonal elements of the Hamiltonian. All relevant information about the bath is contained in the Brownian oscillator spectral density

$$C_{ma,nb}(\omega) = 2\,\mathrm{Im}\int_0^{+\infty} dt \exp(i\omega t)\langle q_{ma}^{(C)}(t) q_{nb}^{(C)}(0)\rangle$$

$$= 2\lambda_{manb}\frac{\omega\Lambda}{\omega^2+\Lambda^2}, \tag{6}$$

where λ_{manb} is the strength and Λ^{-1} is the time scale of bath fluctuations.[34,36]

The last term in the Hamiltonian represents the interaction of the vibrations with the optical field. In the dipole approximation the polarization operator $\hat{\mathbf{P}}$ can be expressed as

$$\hat{\mathbf{P}} = \sum_{ma} \boldsymbol{\mu}_{ma}(\hat{B}_{ma}+\hat{B}_{ma}^{\dagger}) + \boldsymbol{\mu}_{m,ab}\hat{B}_{ma}^{\dagger}\hat{B}_{mb}, \tag{7}$$

$\boldsymbol{\mu}_{ma}$ is the transition dipole moment between the ground state and the excited state a of the mth chromophore, whereas $\boldsymbol{\mu}_{m,ab}$ is the transition dipole between the excited states b and a of the same chromophore.

In our simulations we assumed two identical three level anharmonic vibrations with parameters similar to those of Ref. 37 (see Fig. 1). Excited state energies are Ω_{ma} and Ω_{mb}, and the coupling between the lowest excited states is $J_{ma,na}$. The system has two singly-excited Frenkel exciton states (related to the excitation of molecular states a) with the energies $\Omega_{ma}-J_{ma,na}$ and $\Omega_{ma}+J_{ma,na}$. The lowest excited state is dark, i.e., has zero transition dipole to the ground state, while the higher state has the transition dipole moment $\sqrt{2}\mu_a$. The linear absorption (Fig. 1) consists of the single allowed exciton transition. The higher excited states are two overtone states, $|mb\rangle$, and one double exciton state (combination band) with energy $2\Omega_{ma}$. The resonant transitions relevant for the photon-echo experiment involve these optically allowed states.

The third order polarization created by two optical pulses polarized along $\sigma=z$ was simulated by numerical solution of the nonlinear exciton equations (NEE),[38] which are coupled equations of four types of dynamic variables $B_{ma} = \langle\hat{B}_{ma}\rangle$, $Y_{ma,nb}=\langle\hat{B}_{ma}\hat{B}_{nb}\rangle$, $N_{ma,nb}=\langle\hat{B}_{ma}^{\dagger}\hat{B}_{nb}\rangle$, and $Z_{ma,nb,kc}=\langle\hat{B}_{ma}^{\dagger}\hat{B}_{nb}\hat{B}_{kc}\rangle$. The interaction with the bath results in line broadening and is described using relaxation superoperators in the NEE. We have computed the two-pulse photon echo signal generated in the direction $\mathbf{k}_I=2\mathbf{k}_2-\mathbf{k}_1$ (setting $\mathbf{k}_3=\mathbf{k}_2$). The signal was expressed as a function of the two delay times $P_z^{(3)}(\mathbf{k}_s,t)=P_z^{(3)}(\mathbf{k}_s,\tau_{21},\tau_{42})$, where $\tau_{21}\equiv\bar{\tau}_2-\bar{\tau}_1$ is the delay between the two pulses and $\tau_{42}\equiv\bar{\tau}_4-\bar{\tau}_2$ is the delay between the second pulse and the detection. The signal is displayed as a correlation plot in the frequency domain,
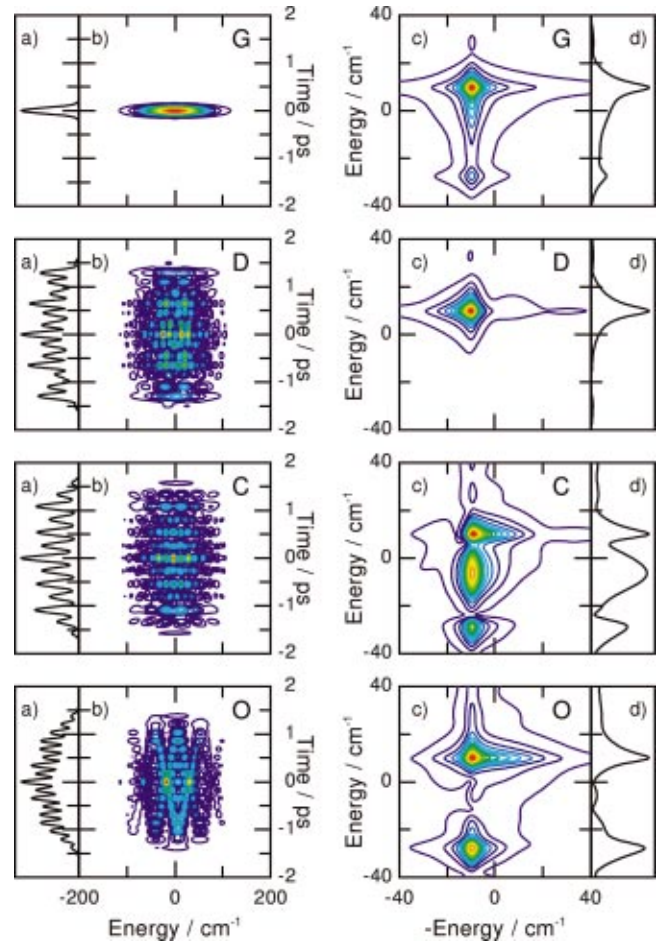

FIG. 2. (Color) Wigner spectrograms of the second optical pulse and the corresponding photon-echo signal $F(\omega_1,\omega_3)$ of the system. Each row corresponds to one nonlinear experiment. The top row shows the results for the Gaussian pulse. The right panel gives the 2D spectrum ($-\omega_1$ vs ω_3) (c) together with the corresponding $\omega_1=10\ \mathrm{cm}^{-1}$ slice along ω_3 axes (d). The left panel shows the Wigner spectrograms of the second pulse (b) and it temporal profile (a) obtained integrating the Wigner spectrogram over the frequency. The following rows shows corresponding the corresponding data for the optimized pulses: (D) diagonal peak maximized; (C) combination band optimized; (O) overtone band optimized. All energies are computed with respect to $\Omega_{ma}=1677\ \mathrm{cm}^{-1}$. The optimal field parameters for diagonal peak are: $c_1=-3.21381$, $c_2=-3.30351$, $c_3=903.531$ fs, $c_4=-0.40409$; for combination peak: $c_1=2.69819$, $c_2=-3.31746$, $c_3=542.42$ fs, $c_4=-1.28757$; for overtone peak: $c_1=-0.23587$, $c_2=3.49987$, $c_3=343.075$ fs, $c_4=2.7182$.

$$F(\omega_1,\omega_3)\equiv\left|\int_0^{\infty}d\tau_{21}\int_0^{\infty}d\tau_{42}\right.$$

$$\left.\times P_z^{(3)}(\mathbf{k}_I,\tau_{21},\tau_{42})\exp(i\omega_1\tau_{21}+i\omega_3\tau_{42})\right|. \tag{8}$$

III. CONTROLLING THE DIAGONAL, OVERTONE, AND COMBINATION BANDS OF COUPLED VIBRATIONS

The frequencies $\bar{\omega}_1$ and $\bar{\omega}_2$ were tuned to the transition frequency of the isolated chromophores Ω_{ma} and both pulses were taken to be Gaussian with widths $\sigma_G=200$ fs (see Appendix). The time and frequency profiles of the pulses may be visualized by displaying their Wigner spectrogram,

$$I_W(\tau,\omega)=\left|\int_{-\infty}^{+\infty}dsE^*(\tau-s/2)(\tau+s/2)e^{i\omega s}\right|. \quad (9)$$

The spectrogram of our Gaussian pulses is shown in the left column top row panel in Fig. 2. We also show its temporal profile $|E(\tau)|^2$ given by the frequency integral of the spectrogram (known as a marginal).

$F(\omega_1,\omega_3)$ was simulated by varying the time intervals τ_{21}, τ_{42} between 0–50 ps in $\Delta\tau=250$ fs increments creating a grid of 200×200 points. The time step for integrating the NEE equations was 200 fs in the absence of optical field and 50 fs when the field is present. This is much shorter than the oscillation period of polarization envelope (200 fs$<\sim3$ ps) and of the optical field envelope (50 fs$<\sim300$ fs). The photon echo spectrum of an ideal system with narrow spectral lines should have three peaks: the diagonal peak (D) $(\omega_1^D,\omega_3^D)=(10\,\text{cm}^{-1},10\,\text{cm}^{-1})$; the combination two-exciton band (C) $(\omega_1^C,\omega_3^C)=(10\,\text{cm}^{-1},-10\,\text{cm}^{-1})$, and the overtone cross-peak (O) $(\omega_1^O,\omega_3^O)=(10\,\text{cm}^{-1},-26\,\text{cm}^{-1})$ related to double excitations of the individual chromophores.

We assumed room temperature $(k_BT=200\,\text{cm}^{-1})$ and the bath relaxation rate $\Lambda=50$ cm^{-1}. The coupling strengths to the bath correspond to the strong coupling regime $[2\pi\lambda_{ma,ma}=0.25\,\text{cm}^{-1},\ 2\pi\lambda_{mb,mb}=1\,\text{cm}^{-1}\ (a=1,\ b=2)]$ leading to dephasing time (inverse linewidth) $\tau_d\approx5$ ps and overlapping spectral lines. The resulting 2D signal is shown in the top row of Fig. 2 (right column). The broad peaks overlap and the combination band (C) is hidden under the diagonal peak (D).

We next show how the various peaks may be resolved using optimized pulse shapes. To define the cost function which will be maximized we first introduce the integrated intensity of peak j;

$$I_j\equiv\int_{-\delta_1}^{\delta_1}d\omega_1\int_{-\delta_3}^{\delta_3}d\omega_3F(\omega_1+\omega_1^j,\omega_3+\omega_3^j),$$

$$j=D,C,O, \quad (10)$$

where we focused on the three peaks: the diagonal peak I_D at (ω_1^D,ω_3^D), the combination peak I_C at (ω_1^C,ω_3^C), and the overtone peak I_O at (ω_1^O,ω_3^O). The integration intervals are $\delta_1=2$ cm^{-1}, $\delta_3=10$ cm^{-1}. The cost function used to maximize the diagonal peak is then defined as $W_D\equiv I_D/(I_C+I_O)$. Similarly we define cost functions for the other peaks $W_C\equiv I_C/(I_D+I_O)$ and $W_O\equiv I_O/(I_D+I_C)$. The evolutionary algorithm is then applied to search for the optimal shape of the second pulse $\mathbf{k}_2$ which maximizes the particular cost function while the first pulse is kept in its original Gaussian form. Further details and parameters of the optimization algorithm are given in the Appendix.

The signals for the optimized diagonal, combination and overtone peaks are shown in the second, third, and fourth rows of Fig. 2 (right column). The corresponding spectrograms of the optimized second pulse are shown in the left column. We further show a section of the 2D spectra for a particular value of ω_1. The convergence of the cost function with generation number is displayed in Fig. 3. For the diagonal peak optimization, W_D is increased by a factor of 2 and the optimized signal shows only the diagonal peak. For the
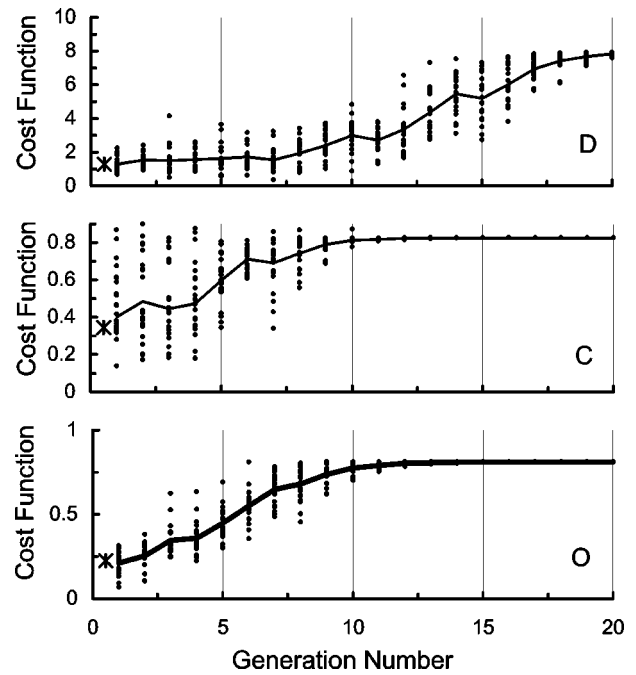

FIG. 3. Distribution of the cost function in the population of genetic algorithm (circles) and its evolution during optimization; solid line shows the average cost value: (D) diagonal peak maximization; (C) combination band optimization; (O) overtone band optimization. The cost value for the initial Gaussian pulses is indicated by a "star."

combination band optimization, W_C is increased almost threefold and the combination peak, which was not resolved prior to optimization, is now clearly visible. The overtone peak is visible even in the case of Gaussian pulses. However W_O is increased by about 3.5 times upon optimization and the signal is better resolved. Figure 3 shows that convergence to the optimal result is fast in all three optimizations and takes 10–20 generations.

IV. DISCUSSION

We have shown how the coherent femtosecond two-dimensional correlation spectrum may be simplified by optimized pulse shapes. The second pulse was optimized to maximize the ratio of the intensity of the diagonal (D), combination (C) or the overtone (O) peaks relative to the other peaks. The ratio was increased two or three times for different peaks and the three peaks are clearly resolved by using shaped pulses. Our simulations demonstrate that the application of shaped optical pulses in coherent nonlinear spectroscopy can reveal otherwise unresolved features, such as the combination peak. The optimal pulse shapes show elaborate time-frequency patterns, as seen in the spectrograms (left column of Fig. 2). These indicate that many frequencies are involved in interference between different elementary transitions or Liouville space pathways.

The ability to control the signal by manipulating phases is intimately connected with the nonlinear response which directly depends on the sum of phases of the fields. Different peaks in the spectrum are controlled through the frequency-dependent phases of the shaped optical pulse. Pulse shaping offers various avenues for interfering the many contributions

to $\chi^{(3)}$, and genetic algorithms provide an affordable way to search the huge parameter space. We have only explored a small fraction of the numerous possibilities offered by Eq. (3) for control: We focused on the $\mathbf{k}_I$ technique and only shaped the second pulse with a limited set of parameters. In the two pulse echo generated in the direction $\mathbf{k}_I = -\mathbf{k}_1 + \mathbf{k}_2 + \mathbf{k}_3$ the second and third pulses are the same and the phase factor is $-i\Phi_1(\omega_a - \bar{\omega}_1) + i\Phi_2(\omega_b - \bar{\omega}_2) + i\Phi_2(\omega_c - \bar{\omega}_2)$. Studying the other techniques $\mathbf{k}_{II} = \mathbf{k}_1 - \mathbf{k}_2 + \mathbf{k}_3$, $\mathbf{k}_{III} = \mathbf{k}_1 + \mathbf{k}_2 - \mathbf{k}_3$, and $\mathbf{k}_{IV} = \mathbf{k}_1 + \mathbf{k}_2 + \mathbf{k}_3$ together with a full scale three pulse optimizations will be most valuable.

Our simulations performed in the weak laser field limit demonstrate the importance of interferences among different coherences [Eq. (3)]. The control could be also improved applying strong saturating laser fields. The Liouville pathways involving saturated populations of the excited states during particular times could contribute significantly to the signal, providing new avenues for control.

Controlling the pulse polarizations by separately shaping the envelopes $\mathcal{E}_{j\alpha}$ with $\alpha = x$, y, z is an exciting new possibility opened up by the pioneering work of Gerber.[7] This should be particularly appealing for the study of chiral systems. Pulse shaped signals combine all tensor components coherently. Circular dichroism (CD) spectra, widely used for characterizing chiral systems probe particular tensor components of $\chi^{(1)}$. Pulses with shaped polarization profiles should provide a novel and unexplored domain of nonlinear spectroscopy, which could provide many more sophisticated means for studying chiral systems with much more detailed information than linear CD spectroscopy. Coherent control algorithms could also be helpful in the design of NMR pulse sequences.[1,2,16] Employing shaped pulses in third order experiments allows not only to resolve the underlying transitions (which can be obtained using tunable narrow band laser sources) but also makes it possible to resolve dynamical processes such as exciton transport and relaxation, charge separation and transfer.

APPENDIX: THE GENETIC ALGORITHM

In this Appendix we briefly describe the pulse parametrization (and shaping) algorithm and the genetic optimization scheme used in our computations.

The envelope function $E_{j\alpha}(\tau)$ ($\tau = t - \bar{\tau}_{j\alpha}$) is parameterized by changing Fourier amplitudes and phases of its direct Fourier transform.[33] The complex time envelope $E_{j\alpha}(\tau)$ is given by

$$E_{j\alpha}(\tau) = W(\tau) \int d\omega \mathcal{E}_{j\alpha}(\omega) \exp[i\phi_{j\alpha}(\omega) - i\omega\tau], \quad \text{(A1)}$$

where $\mathcal{E}_{j\alpha}(\omega)$ and $\phi_{j\alpha}(\omega)$ are real functions. The window-function $W(\tau)$ selects the interval $(-T < \tau < T)$ by adding smooth decay of the field amplitude at the edges of the in-

terval: $W(\tau) = \{\tanh((\tau_w + \tau)/\sigma_w) + \tanh((\tau_w - \tau)/\sigma_w)\}/2$; the parameters τ_w and σ_w define the width of the window and decay rate of the cutoff.

Our search starts with a Gaussian envelope $E_G(\tau) = \exp(-\tau^2/2\sigma_G^2)$. Direct Fourier transform applied to the Gaussian pulse gives $\int d\tau E_G(\tau) \exp(i\omega\tau) \equiv \mathcal{E}_G(\omega) \exp(i\phi_G(\omega))$, where the amplitude $\mathcal{E}_G(\omega)$ and the phase $\phi_G(\omega)$ describe the Gaussian field. The shaped pulse is obtained by adding a frequency dependent phase: $\phi_G(\omega) \Rightarrow \phi_{j\alpha}(\omega) = \phi_G(\omega) + \psi_{j\alpha}(\omega)$, where the additional phase profile $\psi_{j\alpha}(\omega) = c_{1j\alpha} + c_{2j\alpha}\sin(c_{3j\alpha}\omega + c_{4j\alpha})$ is defined by four parameters $c_{uj\alpha}$, ($u = 1,2,3,4$). It is also possible to modulate the amplitude $\mathcal{E}_{j\alpha}(\omega)$, this was not done here and we set $\mathcal{E}_{j\alpha}(\omega) = \mathcal{E}_G(\omega)$.

The initial width of Gaussian pulses was taken to be $\sigma_G = 200$ fs, a time window of 4 ps was considered for the shaped pulse ($T = 2$ ps), $N_f = 128$ frequencies of the Fourier space were used in the Fourier transformation and the window function parameters were accepted as follows: $\tau_w = 1.6$ ps, $\sigma_w = 100$ fs. We used a fixed pulse polarization $\alpha = z$, parallel to the transition dipoles. All quantities in this section refer to this component of the field. We will therefore omit the indices $j\alpha$ in the following.

The genetic algorithm consists of several steps which, adopting evolution theory terminology, are labeled as population-creation, selection, crossing, and mutation.[32] These are defined within the chosen optimization parameter space.

In the first *population-creation* step, an ensemble of N phase profiles (representing N trial optical pulses) is generated randomly. This forms the first generation of pulse population; N is a parameter of the algorithm. Each member of the population corresponds to one point (c_1, c_2, c_3, c_4) in the four-parameter space. In the second, *selection*, step, the cost function is calculated for each population member and the decision whether a selection is accepted is made using the following rule: An integer random number x is generated in the interval $[L_i, L_f]$ and x population members with the lowest cost are selected. The numbers L_i ($L_i < N$) and L_f ($L_i < L_f < N$) are also parameters of the algorithm.

A new generation of the population is created using the selected x members of the first generation while the other, $N - x$, are created from the selected members by means of *crossing*. The following rule draws an integer random number y from the interval $[1, M]$, where M is the number of parameters (4 in our case), select randomly two members (with parameters $c_u^{(1)}$ and $c_u^{(2)}$ respectively), from the selection, and create a new member $c_u^{(3)}$, defined as

$$c_u^{(3)} = \begin{cases} c_u^{(1)}, & u \leq y \\ c_u^{(2)}, & u > y. \end{cases} \quad \text{(A2)}$$

This is known as a single point crossing.

In order to explore the new points of the parameter space, a noise, *mutation*, is added to all parameters of the newly created population. The mutation is added as a shift of the parameter value by a Gaussian random number z with zero mean and the width σ_{mut}. Then, for instance $c_u \Rightarrow c_u + w_{cu}z$, where w_{cu} is a weight factor for the parameter c_u.

The optimization process involves repeating the selection, crossing, mutation sequence, finally leading to an optimized population. In order to narrow down the range of populations in the optimal solution, the noise is reduced (or increased) depending on the average cost of the population on the previous step. The population is evaluated by defining the cost threshold W_{max} and the number of population members N_{bad} with the cost *below* (for maximization—*above* would be for minimization) W_{max}. The decision is then made depending on the ratio $\eta = N_{bad}/N$. If $\eta \leq 0.5$ (population is "good") the cost threshold is increased (reduced) by a factor of 2 (and the noise parameter σ_{mut} is increased by a factor of ϵ to escape possible local minima). For $\eta > 0.5$ the noise parameter σ_{mut} is reduced by the same factor ϵ allowing to narrow the population distribution around the global minima.

Initially the cost threshold is small compared to the possible values of the cost function and the noise parameter is large covering the entire parameter space. Fast exponential convergence was observed for the value $\epsilon = 0.6^{-1}$ which was held constant in all simulations. The population number was $N = 20$ and the parameters of the selection: $L_i = 4$ and $L_f = 6$. Other parameters used are the initial cost threshold $W_{max} = 0.1$, the initial width $\sigma_{mut} = 1$, the weights of the parameters: $w_{c1} = w_{c2} = w_{c4} = 1$, $w_{c3} = 180$. The c parameters were varied in the range c_1, c_2, $c_4 \in (-\pi, \pi)$ and $c_3 \in (0, 1000)$.

[1] R. R. Ernst, G. Bodenhausen, and A. Wokaun, *Principles of Nuclear Magnetic Resonance in One and Two Dimensions* (Oxford University Press, Oxford, 1990).

[2] R. Riek, J. Fiaux, E. B. Bertelsen, A. L. Horwich, and K. Wüthrich, J. Am. Chem. Soc. **124**, 12144 (2002); K. Wüthrich, *NMR of Proteins and Nucleic Acids* (Wiley, New York, 1986).

[3] A. M. Weiner, D. E. Leird, G. P. Weiderrecht, and K. A. Nelson, Science **286**, 1317 (1990).

[4] J. X. Tull, M. A. Dugan, and W. S. Warren, Adv. Magn. Opt. Reson. **20**, 1 (1990).

[5] N. F. Scherer, R. J. Carlson, A. Matro, M. Du, A. J. Rugiero, V. Romero-Rochin, J. A. Cina, G. R. Fleming, and S. A. Rice, J. Chem. Phys. **95**, 1487 (1991).

[6] H. Rabitz, R. de Vivie-Riedle, M. Motzkus, and K. Kompa, Science **288**, 824 (2000).

[7] T. Brixner, G. Krampert, P. Niklaus, and G. Gerber, Appl. Phys. B: Lasers Opt. **74**, S133 (2002); T. Brixner, G. Krampert, P. Niklaus, and G. Gerber, Appl. Phys. B Suppl. **74**, S133S144 (2002); T. Brixner, N. H. Damrauer, G. Krampert, P. Niklaus, and G. Gerber, J. Opt. Soc. Am. B **20**, 878 (2003).

[8] V. V. Lozovoy, I. Pastirk, K. A. Walowicz, and M. Dantus, J. Chem. Phys. **118**, 3187 (2003); M. Dantus, Annu. Rev. Phys. Chem. **52**, 639 (2001).

[9] P. Tian, D. Keusters, Y. Suzaki, and W. S. Warren, Science **300**, 1553 (2003).

[10] S. Mukamel, Annu. Rev. Phys. Chem. **51**, 691 (2000).

[11] S. Mukamel and R. M. Hochstrasser, editors, "Special Issue on Multidimensional Spectrocopies," Chem. Phys. **266**, No. 2/3 (2001).

[12] D. S. Larsen, K. Ohta, Q. H. Xu, M. Cyrier, and G. Fleming, J. Chem. Phys. **114**, 8008 (2001); K. Ohta, D. S. Larsen, M. Yang, and G. Fleming, *ibid.* **114**, 8020 (2001).

[13] P. Hamm and R. M. Hochstrasser, *Structure and Dynamics of Proteins and Peptides: Femtosecond Two-Dimensional Spectroscopy, Ultrafast Infrared and Raman Spectroscopy*, edited by M. D. Fayer (Marcel Dekker, New York, 2001).

[14] P. Hamm, M. Lim, W. F. DeGrado, and R. M. Hochstrasser, J. Chem. Phys. **112**, 1907 (2000).

[15] M. Khalil and A. Tokmakoff, Chem. Phys. **266**, 213 (2001).

[16] F. Delaglio, G. Kontaxis, and A. Bax, J. Am. Chem. Soc. **122**, 2142 (2000); G. Barbato, M. Ikura, L. E. Kay, R. W. Pastor, and A. Bax, Biochemistry **31**, 5269 (1992).

[17] C. Scheurer and S. Mukamel, J. Chem. Phys. **115**, 4989 (2001); **116**, 6803 (2002).

[18] R. J. Levis and H. A. Rabitz, J. Phys. Chem. A **106**, 6427 (2002).

[19] H. Rabitz and W. Zhu, Acc. Chem. Res. **33**, 572 (2000).

[20] D. J. Tannor and S. A. Rice, Adv. Chem. Phys. **70**, 441 (1988); P. Gaspard and J. Burghardt, editors, *Chemical Reactions and Their Control on the Femtosecond Time Scale*, Adv. Chem. Phys. **101** (1997).

[21] R. Plass, K. Egan, C. Collazo-Davila, D. Grozea, E. Landree, L. D. Marks, and M. Gajdardziska-Josifovska, Phys. Rev. Lett. **81**, 4891 (1998).

[22] J. H. Kiefer, K. I. Mitchell, R. D. Kern, and J. N. Yong, J. Phys. Chem. **92**, 677 (1988).

[23] J. Stippler, C. Schlichenmaier, A. Knorr, T. Meier, M. Lindberg, P. Thomas, and S. W. Koch, Phys. Status Solidi B **221**, 379 (2000).

[24] J. L. Herek, W. Wohlleben, R. J. Cogdell, D. Zeidler, and M. Motzkus, Nature (London) **417**, 533 (2002).

[25] T. Hornung, R. Meier, R. de Vivie-Riedle, and M. Motzkus, Chem. Phys. **267**, 261 (2001).

[26] D. Meshulach and Y. Silberberg, Nature (London) **396**, 239 (1998).

[27] T. Hornung, R. Meier, D. Zeidler, K.-L. Kompa, D. Proch, and M. Motzkus, Appl. Phys. B: Lasers Opt. **71**, 277 (2000).

[28] R. Bartels, S. Backus, E. Zeek, L. Misoguti, G. Vdovin, I. P. Christov, M. M. Muriname, and H. C. Kaptein, Nature (London) **406**, 164 (2000).

[29] N. Dudovich, D. Oron, and Y. Silberberg, Nature (London) **418**, 512 (2002).

[30] D. Oron, N. Dudovich, D. Yelin, and Y. Silberberg, Phys. Rev. A **65**, 043407 (2002).

[31] R. S. Judson and H. Rabitz, Phys. Rev. Lett. **68**, 1500 (1992).

[32] D. E. Goldberg, *Genetic Algorithms in Search, Optimization, and Machine Learning* (Addison-Wesley, Reading, 1989).

[33] D. Zeidler, S. Frey, K.-L. Kompa, and M. Motzkus, Phys. Rev. A **64**, 023420 (2001).

[34] S. Mukamel, *Principles of Nonlinear Optical Spectrscopy* (Oxford University Press, New York, 1995).

[35] K. Ohta, M. Yang, and G. Fleming, J. Chem. Phys. **115**, 7609 (2001).

[36] V. Chernyak and S. Mukamel, J. Chem. Phys. **105**, 4565 (1996).

[37] A. Piryatinski, V. Chernyak, and S. Mukamel, Chem. Phys. **266**, 285 (2001).

[38] V. Chernyak, W. M. Zhang, and S. Mukamel, J. Chem. Phys. **109**, 9587 (1998).